Theoretical Analysis of the Magnetic Freedericksz Transition in the Presence of Flexoelectricity and Ionic Contamination

Running title: Magnetic Freedericksz Transition

A.A.T. Smith[1], C.V. Brown[1] and N.J. Mottram[2]

[1]School of Biomedical and Natural Sciences,
Nottingham Trent University,
Erasmus Darwin Building,
Clifton Lane, Clifton,
Nottingham, NG11 8NS,
United Kingdom

[2]Department of Mathematics,
University of Strathclyde,
Livingstone Tower,
26 Richmond Street,
Glasgow, G1 1XH,
United Kingdom

January 31, 2007

keywords:

PACS Numbers: 77. (Dielectrics, piezoelectrics, and ferroelectrics and their properties), 77.22.Ch (Permittivity (dielectric function)), 77.84.Nh (Liquids, emulsions, and suspensions; liquid crystals), 75. (Magnetic properties and materials), 75.30.Gw (Magnetic anisotropy).

E-mail: carl.brown@ntu.ac.uk, Tel: +44-(0)115-848-3184; Fax: +44-(0)115-848-6636

Abstract

We have derived an approximate analytical expression for the static director distortion of a planar nematic layer subject to a magnetic field H immediately above the critical Freedericksz transition $H = H_c$. The layer contains a voltage-independent density of positively and negatively singly charged ionic species that interact with the flexoelectric and dielectric polarisations which appear when the director is distorted. The analytical solution is shown to correspond closely to a full numerical calculation when $H/H_c = 1.01$. The analytical approach allows a quantitive insight into how the mobile charge shields the polarisation for different values of the elastic constants, the ionic density, the flexoelectric coefficients and the layer thickness.

1 Introduction

Nematic liquid crystal materials generally contain molecules that possess permanent dipole moments and that also exhibit an anisotropic electronic polarisability and an anisotropic diamagnetic susceptability. The average molecular orientation in the nematic phase is described by the director, **n**. Due to the symmetry of the molecular ordering the phase exhibits dielectric and magnetic anisotropies, with different values of the permittivity and the susceptability observed parallel to and perpendicular to the **n**-director, but there is no spontaneous bulk polarisation of the phase [1, 2].

In 1969 Meyer [3] proposed that a bulk polarisation would arise from distortions in the **n**-director if the nematic molecules possessed a shape polarity as well as a permanent electric dipole moment. This effect, which has become known as the flexoelectric effect, is analogous to the piezoelectric effect in certain crystals. The flexoelectric effect has been observed in polar nematics and also for nematic materials for which the molecules are non-polar and symmetric. In the latter case the appearance of the flexoelectric polarisation was attributed to the contribution from a molecular quadrapole moment [4, 5].

Measurement of the Freedericksz transition of a nematic layer induced by a magnetic field or an a.c. voltage has become an established technique for the determination of the values of the Frank-Oseen elastic constants of nematic liquid crystal materials [6, 7, 8, 9]. For example, a planar aligned nematic layer will undergo a splay distortion when a magnetic field above the critical value $H = H_c$ is applied normal to the layer as long as the magnetic susceptability parallel to the **n**-director, $\chi_{\parallel}$, is larger than the value perpendicular to the **n**-director, $\chi_{\perp}$, so that $\Delta\chi = \chi_{\parallel} - \chi_{\perp} > 0$. There is no distortion below $H = H_c$ but the magnitude of the distortion, which can be quantified in terms of the mid-layer tilt angle θ_m, increases sharply as the magnetic field is increased above the critical value.

In 1974 Deuling [10] reported a theoretical investigation into the influence of a flexoelectric polarisation on the magnetic Freedericksz effect. Increasing the magnitude of the sum of the flexoelectric coefficients, $e_{11} + e_{33}$, does not shift the critical field H_c but it does decrease the gradient of the mid layer tilt as a function of magnetic field immediately above the threshold. This "flexoelectric stiffening" was also implicity predicted to occur from analysis of the Freedericksz effect induced by electric fields in the presence of a flexoelectric polarisation [11]. More recent work by the present authors on the a.c. electrically induced Freedericksz transition considered the near "degeneracy" of the effect on the static distortion of the **n**-director profile between decreasing the value of the nematic elastic constant ratio K_3/K_1 and increasing the value of $e_{11} + e_{33}$ when fitting the shape of the capacitance-voltage curve above the threshold voltage [12].

Historically, different measurement approaches have disagreed in the magnitude and even sign of the flexoelectric coefficients when applied to the same material (e.g. 5CB or MBBA) [13]. One reason for this is the presence of mobile ionic contamination. When measure-

ments are made with a magnetic field or with an a.c. electric field whose period is shorter than the space charge relaxation time there will be an ion-director-polarisation coupling. The effect is most marked in polar nematic materials and when the measurement geometry is itself asymmetric, for instance the hybrid aligned nematic geometry. Ponti [14] first demonstrated that both the sign and magnitude of $e_{11}+e_{33}$ was changed when the data of [15] was refitted with an ionic charge number density of 1.0×10^{20} m^{-3}.

In this paper a theoretical investigation is presented of the magnetically induced Freedericksz transition in the planar or "splay" alignment geometry. Equations describing nematic continuum theory, non-equilibrium charge transport, and the appropriate Maxwell's equations of electromagnetism are solved self consistently in order to investigate how the flexoelectric polarisation of the distorted layer can be shielded by the mobile ionic charge.

2 Model and Governing Equations

The geometry that will be investigated consists of two parallel plates with the liquid crystal sandwiched between them as depicted in Fig. 1. The director tilt angle θ is defined relative to the confining plates as shown in the Fig. 1. It will be assumed that the **n**-director lies parallel to the boundaries at both of the surfaces, so that $\theta(z=0)=\theta(z=d)=0$ rad. A magnetic field **H** is applied perpendicular to the cell and, since the magnetic susceptability anisotropy $\Delta\chi$ is assumed to be positive, director re-orientation is expected to occur once the field exceeds some critical threshold value $|\mathbf{H}|=H_c$. The flexoelectric polarisation, which is obtained as a direct consequence of this induced director distortion, then creates an internal electric field **E**. This acts in such a way so as to essentially reduce the effect of the magnetic field. It will be assumed that two types of mobile ionic species are present in the layer simultaneously, one having charge $+|e|$ and number density n_h, and the other having charge $-|e|$ and number density n_e. The positively charged ionic species will be referred to as "holes" and the negatively charged ionic species as "electrons" (these labels have no physical significance but are used simply to aid the brevity and flow of the article).

From liquid crystal continuum theory [16, 17, 18, 19] the total free energy density in such a cell is given by

$$\begin{aligned} w &= w_{elastic}+w_{magnetic}+w_{electric} \\ &= w_{elastic}+w_{magnetic}+(w_{dielectric}+w_{flexoelectric}+w_{ionic}) \\ &= \tfrac{1}{2}K_1\left(\nabla\cdot\mathbf{n}\right)^2+\tfrac{1}{2}K_2\left(\mathbf{n}\cdot\nabla\times\mathbf{n}\right)^2+\tfrac{1}{2}K_3\left(\mathbf{n}\times\nabla\times\mathbf{n}\right)^2 \\ &\quad +\tfrac{1}{2}\left(K_2+K_4\right)\nabla\cdot\left[\left(\mathbf{n}\cdot\nabla\right)\mathbf{n}-\left(\nabla\cdot\mathbf{n}\right)\mathbf{n}\right]-\tfrac{1}{2}\mu_0\Delta\chi\left(\mathbf{n}\cdot\mathbf{H}\right)^2 \\ &\quad -\tfrac{1}{2}\epsilon_0\epsilon_\perp E^2-\tfrac{1}{2}\epsilon_0\epsilon_a\left(\mathbf{n}\cdot\mathbf{E}\right)^2-e_{11}\left(\nabla\cdot\mathbf{n}\right)\left(\mathbf{n}\cdot\mathbf{E}\right)+e_{33}\left(\mathbf{n}\times\nabla\times\mathbf{n}\right)\cdot\mathbf{E}+\rho_f U \end{aligned} \quad (1)$$

where the K_i are the usual Frank elastic constants, μ_0 and ϵ_0 are the permeability and permittivity of free space, e_{11} and e_{33} are the splay and bend flexoelectric coefficients, respectively,

$\rho_f = |e|(n_h - n_e)$ is the free charge density and U denotes the electric potential. The unitless constant $\epsilon_a = \epsilon_{\|} - \epsilon_{\perp}$ is the dielectric anisotropy of the material with $\epsilon_{\|}$ and $\epsilon_{\perp}$ being the relative dielectric permittivities parallel and perpendicular to the **n**-director. Due to the symmetry of the geometry it will reasonably be assumed that the director distortion angle θ, electric field magnitude $E = |\mathbf{E}|$ and the electron and hole number densities (n_e and n_h) are spatially only dependent on z. This allows us to introduce the following:

$$\mathbf{H} = (0, 0, H), \quad \mathbf{E} = (0, 0, E(z,t)), \quad \mathbf{n} = (\cos\theta(z,t), 0, \sin\theta(z,t)), \tag{2}$$

where H is assumed constant over the cell. Inserting these into equation (1) and writing the electric field in terms of the potential via the relation $\mathbf{E} = -\nabla U$ [20] then gives the total free energy density to be

$$\begin{aligned} w &= \frac{1}{2}\left[K_1\cos^2\theta + K_3\sin^2\theta\right]\left(\frac{\partial\theta}{\partial z}\right)^2 - \frac{1}{2}\mu_0\Delta\chi H^2\sin^2\theta \\ &\quad -\frac{1}{2}\epsilon_0\left(\epsilon_\perp + \epsilon_a\sin^2\theta\right)\left(\frac{\partial U}{\partial z}\right)^2 + (e_{11}+e_{33})\sin\theta\cos\theta\left(\frac{\partial\theta}{\partial z}\right)\left(\frac{\partial U}{\partial z}\right) + \rho_f U. \end{aligned} \tag{3}$$

The next step is to minimise the total energy of the system in order to obtain the governing differential equation for the director distortion angle. Using the calculus of variations [18] this process leads to the equation

$$\begin{aligned} &\left(K_1\cos^2\theta + K_3\sin^2\theta\right)\left(\frac{\partial^2\theta}{\partial z^2}\right) + \frac{1}{2}(K_3 - K_1)\sin(2\theta)\left(\frac{\partial\theta}{\partial z}\right)^2 + \frac{1}{2}\epsilon_0\epsilon_a\sin(2\theta)\left(\frac{\partial U}{\partial z}\right)^2 \\ &+\frac{1}{2}(e_{11}+e_{33})\sin(2\theta)\left(\frac{\partial^2 U}{\partial z^2}\right) + \frac{1}{2}\mu_0\Delta\chi H^2\sin(2\theta) - \gamma_1\left(\frac{\partial\theta}{\partial t}\right) = 0, \end{aligned} \tag{4}$$

where γ_1 represents the director rotational viscosity. In addition to the above it is also essential to ensure that Maxwell's equations for electric and magnetic fields are simultaneously satisfied. In this situation, where the magnetic field is considered to be constant in both space and time, and it is assumed that $\mathbf{E} = -\nabla\mathbf{V}$ the only Maxwell equation that needs to be explicitly solved is $\nabla\cdot\mathbf{D} = \rho_f$ where $\mathbf{D}$ is the electric displacement which can be expressed as [1]

$$\mathbf{D} = \epsilon_0\epsilon_\perp\mathbf{E} + \epsilon_0\epsilon_a(\mathbf{n}\cdot\mathbf{E})\mathbf{n} + e_{11}(\nabla\cdot\mathbf{n})\mathbf{n} - e_{33}(\mathbf{n}\times\nabla\times\mathbf{n}), \tag{5}$$

which upon insertion into the Maxwell equation leads to the differential equation

$$\frac{\partial}{\partial z}\left[-\epsilon_0\epsilon_\perp\left(\frac{\partial U}{\partial z}\right) - \epsilon_0\epsilon_a\sin^2\theta\left(\frac{\partial U}{\partial z}\right) + \frac{1}{2}(e_{11}+e_{33})\sin(2\theta)\left(\frac{\partial\theta}{\partial z}\right)\right] = |e|(n_h - n_e). \tag{6}$$

In order to model the ion distribution the non-equilibrium charge transport equations must also be solved:

$$\frac{\partial n_e}{\partial t} + \mu_e\frac{\partial}{\partial z}\left[n_e\frac{\partial U}{\partial z} - \frac{D_e}{\mu_e}\frac{\partial n_e}{\partial z}\right] = 0, \quad \frac{\partial n_h}{\partial t} - \mu_h\frac{\partial}{\partial z}\left[n_h\frac{\partial U}{\partial z} + \frac{D_h}{\mu_h}\frac{\partial n_h}{\partial z}\right] = 0, \tag{7}$$

where μ_e and μ_h are the electron and hole mobilities and D_e and D_h are the electron and hole diffusivities. Temperature activated effects such as generation-recombination due to the dynamic equilibrium between neutral molecules and dissociated ion-pairs are not considered in the present model [21].

For the analytical work it is being assumed that the "strong anchoring" condition holds at the boundaries $z = 0$ and $z = d$ which means that the director is fixed parallel to the surfaces. It is necessary to introduce a very small initial tilt angle throughout the bulk of the layer when the system is modelled numerically. Additionally, since no external electric field is being applied we assume that the bounding plates are both held at zero potential. For the charge transport equations we consider the boundaries to be insulated meaning that no current can flow into or out of the cell. Since the boundaries are earthed but allow no charge flow they can be regarded as unreactive or passivated. This approximates to the situation in a practical device where the electrodes are coated with a thin dielectric layer. Mathematically, these conditions can be expressed in the forms:

$$\begin{aligned} &\theta(0,t) = \theta(d,t) = 0, \quad n_e(z,t)\left.\frac{\partial U(z,t)}{\partial z}\right|_{z=0,d} - \frac{D_e}{\mu_e}\left.\frac{\partial n_e(z,t)}{\partial z}\right|_{z=0,d} = 0, \\ &U(0,t) = U(d,t) = 0, \quad n_h(z,t)\left.\frac{\partial U(z,t)}{\partial z}\right|_{z=0,d} + \frac{D_h}{\mu_h}\left.\frac{\partial n_h(z,t)}{\partial z}\right|_{z=0,d} = 0. \end{aligned} \tag{8}$$

In addition to the boundary conditions discussed above, we also require the following initial conditions:

$$\theta(z,0) = 0, \quad U(z,0) = 0, \quad n_e(z,0) = n_h(z,0) = n_0 \tag{9}$$

It is therefore assumed that at $t = 0$ the charge is uniformly distributed with a known density which means that n_0 is constant.

3 Analytical Solution

Although the full system of equations defined by (4), (6) and (7), along with their associated boundary and initial conditions (8) and (9) can be solved numerically, an analytical solution provides some insight into the precise relation between the director orientation and the various field components. In this section we derive an approximate asymptotic static solution when the applied magnetic field is just above the threshold. We introduce a small perturbation parameter, ϵ through the relation

$$H = H_c\left(1 + \epsilon^2\right), \tag{10}$$

and construct series solutions of the form

$$\begin{aligned} \theta &= \epsilon\theta_1 + \epsilon^3\theta_3 + \ldots, \quad n_e = n_0 + \epsilon^2 n_{e2} + \epsilon^4 n_{e4} + \ldots, \\ U &= \epsilon^2 U_2 + \epsilon^4 U_4 + \ldots, \quad n_h = n_0 + \epsilon^2 n_{h2} + \epsilon^4 n_{h4} + \ldots. \end{aligned} \tag{11}$$

Inserting these into the governing equations (4), (6) and (7) and making use of the approximations

$$\sin^2\theta \approx \theta^2 - \tfrac{1}{3}\theta^4, \quad \sin(2\theta) \approx 2\theta - \tfrac{4}{3}\theta^3, \tag{12}$$

we obtain, up to third order in ϵ, the following system of differential equations:

$$\begin{aligned}\left[K_1\theta_{1zz} + \mu_0\Delta\chi H_c^2\theta_1\right]\epsilon + \left[K_1\theta_{3zz} - K_1\theta_1^2\theta_{1zz} + K_3\theta_1^2\theta_{1zz} + (K_3 - K_1)\,\theta_1\theta_{1z}^2\right.\\ \left. + (e_{11} + e_{33})\,\theta_1 U_{2zz} + \mu_0\Delta\chi H_c^2\theta_3 - \tfrac{2}{3}\mu_0\Delta\chi H_c^2\theta_1^3 + 2\mu_0\Delta\chi H_c^2\theta_1\right]\epsilon^3 = 0,\end{aligned} \tag{13}$$

$$\left[-\epsilon_0\epsilon_\perp U_{2z} + (e_{11} + e_{33})\,\theta_1\theta_{1z}\right]_z \epsilon^2 = |e|\,(n_{h2} - n_{e2})\,\epsilon^2, \tag{14}$$

$$\left[-\frac{D_e}{\mu_e}n_{0z}\right]_z + \left[n_0 U_{2z} - \frac{D_e}{\mu_e}n_{e2z}\right]_z \epsilon^2 = 0, \tag{15}$$

$$\left[\frac{D_h}{\mu_h}n_{0z}\right]_z + \left[n_0 U_{2z} + \frac{D_h}{\mu_h}n_{h2z}\right]_z \epsilon^2 = 0, \tag{16}$$

where the z subscripts denote differentiation. These equations are now solved sequentially, for each power of ϵ, making use of the boundary conditions in (8).

It is clear to see that the zeroth order equations are trivially satisfied since n_o is a constant and the only first order equation arises from (13). Solving this gives rise to the familiar threshold expression

$$H_c = \frac{\pi}{d}\sqrt{\frac{K_1}{\mu_0\Delta\chi}}, \tag{17}$$

along with the solution term

$$\theta_1 = B\sin\left(\frac{\pi z}{d}\right), \tag{18}$$

where B is a constant of integration, yet to be determined. Turning to the second order equations, it is now possible to simulatenously solve (14), (15) and (16) to obtain the solutions

$$\begin{aligned}U_2 &= \left(\frac{\sigma(D-C) - \eta B^2}{1 + \exp(\lambda d)}\right)\exp(\lambda z) + \eta B^2\cos\left(\frac{2\pi z}{d}\right) + \sigma(C - D)\\ &\quad + \left[\sigma(D-C) - \eta B^2 - \left(\frac{\sigma(D-C) - \eta B^2}{1 + \exp(\lambda d)}\right)\right]\exp(-\lambda z),\end{aligned} \tag{19}$$

$$\begin{aligned}n_{e2} &= +\frac{\mu_e n_0}{D_e}\left\{\left[\sigma(D-C) - \eta B^2 - \left(\frac{\sigma(D-C) - \eta B^2}{1 + \exp(\lambda d)}\right)\right]\exp(-\lambda z)\right.\\ &\quad \left. + \left(\frac{\sigma(D-C) - \eta B^2}{1 + \exp(\lambda d)}\right)\exp(\lambda z) + \eta B^2\cos\left(\frac{2\pi z}{d}\right) + \sigma(C - D)\right\} + C,\end{aligned} \tag{20}$$

$$\begin{aligned}n_{h2} &= -\frac{\mu_h n_0}{D_h}\left\{\left[\sigma(D-C) - \eta B^2 - \left(\frac{\sigma(D-C) - \eta B^2}{1 + \exp(\lambda d)}\right)\right]\exp(-\lambda z)\right.\\ &\quad \left. + \left(\frac{\sigma(D-C) - \eta B^2}{1 + \exp(\lambda d)}\right)\exp(\lambda z) + \eta B^2\cos\left(\frac{2\pi z}{d}\right) + \sigma(C - D)\right\} + D,\end{aligned} \tag{21}$$

where C and D are integration constants and we have introduced the parameters

$$\lambda = \sqrt{\frac{|e|\, n_0}{\epsilon_0 \epsilon_\perp}\left(\frac{\mu_h}{D_h} + \frac{\mu_e}{D_e}\right)}, \quad \eta = -\frac{(e_{11} + e_{33})\,\pi^2}{\epsilon_0 \epsilon_\perp d^2} \Bigg/ \left(\frac{4\pi^2}{d^2} + \lambda^2\right), \quad \sigma = -\frac{|e|}{\epsilon_0 \epsilon_\perp \lambda^2}. \tag{22}$$

Due to the insulating boundary conditions, no charge can either enter or leave the cell and as we have assumed that there are no charge generation or recombination processes ocurring we can consider the total amount of each type of charge to be conserved within the cell. Since the leading order terms of the electron and hole number density series solutions are equal to the constant initial density n_0 we can assume that each of the remaining terms must integrate to zero. Applying this condition to equations (20) and (21) gives two of the integration constants to be

$$C = \frac{\mu_e n_0 \eta B^2}{D_e}, \quad D = -\frac{\mu_h n_0 \eta B^2}{D_h} \tag{23}$$

Next, in order to obtain the constant B, we turn to the third order term of the differential equation (13) where detailed, but straightforward, calculations eventually yield

$$B = \left\{ \frac{K_3}{4K_1} + \frac{(e_{11} + e_{33})^2\, \pi^2}{K_1 \epsilon_0 \epsilon_\perp \left(4\pi^2 + \lambda^2 d^2\right)} \right\}^{-1/2}. \tag{24}$$

It should be noted that a negative solution for B also exists, however this just corresponds to a rotation of the director in the opposite direction. The solutions up to second order in ϵ may now be simplified to reveal that

$$\theta = \epsilon B \sin\left(\frac{\pi z}{d}\right), \tag{25}$$

$$U = \eta B^2 \left[\cos\left(\frac{2\pi z}{d}\right) - 1\right] \epsilon^2, \tag{26}$$

$$n_e = n_0 + \frac{\mu_e n_0}{D_e} \eta B^2 \cos\left(\frac{2\pi z}{d}\right) \epsilon^2, \tag{27}$$

$$n_h = n_0 - \frac{\mu_h n_0}{D_h} \eta B^2 \cos\left(\frac{2\pi z}{d}\right) \epsilon^2. \tag{28}$$

It can also be shown that, when $n_0 = 0$, the expression for the maximum distortion angle, $\theta_m = \epsilon B$, reduces to that obtained elsewhere [11, 22] when ions are not considered. Additionally, in the absence of both flexoelectricity and ionic contamination it simplifies to the analytic solution found in the literature [18].

4 Results

In order to check the accuracy of the analytic solution we have solved the full set of differential equations (4), (6) and (7), subject to the conditions (8) and (9), numerically using the finite

element package COMSOL Multiphysics [23]. Although the full dynamic equations were used for these solutions, only the final static state results are presented here.

Unless stated otherwise the parameter values used are those displayed in Table 1. Here we have used measurements performed on the material E7 for the permittivity components and elastic constants and $\Delta\chi$ takes on a typical value for nematic materials [12, 18]. The diffusivity constants are calculated using the Einstein relation $D = \mu k_B T/|e|$ where k_B denotes the Boltzmann constant, and the temperature T was assumed to be 300 K. An unusually small viscosity vaue was used to reduce computational time for the numerical solutions. This does not have any consequences for the static solutions in which we are interested.

In Figs. 2 and 3 we show a comparison of the analytical solutions, obtained using equations (25) to (28), and those computed numerically for the director distortion angle, potential and ion number densities across the cell at two different applied magnetic field strengths. The dashed lines correspond to the predictions of the analytical solution and the solid lines to the predictions of the full numerical calculations. When the magnetic field is just above the threshold, $H/H_c = 1.01$, there is close agreement between the numerical and analytical solutions. The deviation between the two solutions becomes significant at higher fields, when $H/H_c = 1.05$, as a result of limiting the asymptotic analysis to second order in ϵ. The magnitude of the flexoelectric polarisation will be higher in the regions where there are spatial gradients in the **n**-director angle θ and the potential U, as can be seen from equation (1). In Fig. 3 the mobile positive and negative charges react oppositely to the variation of the polarisation through the layer with the number density of electrons being enhanced at the centre of the cell, but depleted near to the boundaries, whereas the number density of holes is enhanced near to the boundaries, but depleted towards the centre.

Figure 4 illustrates the effects that both flexoelectricity and ionic contamination can have on the **n**-director distortion angle through the cell when $H/H_c = 1.5$. These data and the data for all subsequent graphs have been obtained through numerical solution of equations (4), (6) and (7). The solid line shows the distortion that has been calculated in the absence of any ionic contamination or flexoelectric polarisation when $n_o = 0$ m^{-3} and $e_{11}+e_{33} = 0$ Cm^{-1}. The mid-layer tilt angle is $\theta_m = 1.036$ rad. If the ionic number density is maintained at zero but the flexoelectric polarisation is increased to $e_{11} + e_{33} = 3.0 \times 10^{-11}$ Cm^{-1} the distortion decreases and there is a significant reduction in the mid-layer tilt angle, now $\theta_m = 0.984$ rad. This effect has been previously reported and investigated [10].

The effect of increasing the charge number density is then investigated for the case where the sum of the flexoelectric coefficients is kept constant at $e_{11} + e_{33} = 3.0 \times 10^{-11}$ Cm^{-1}. For $n_o = 1.0 \times 10^{17}$ m^{-3} the difference from the **n**-director distortion profile for when $n_o = 0.0$ m^{-3} is negligible. If this profile was plotted in Fig. 4 it would therefore be coincident with the lower dotted curve. When the number density is increased further the mobile ionic species begin to shield the flexoelectric polarisation and the reduction in the mid-layer tilt angle relative to when the sum of the flexoelectric coefficients is zero is not as marked. The curve

for $n_o = 1.0 \times 10^{19}$ m^{-3} and $e_{11} + e_{33} = 3.0 \times 10^{-11}$ Cm^{-1}, shown as the alternate dot-dashed curve in Fig. 4 lies only just below the solid curve in Fig. 4 for which $n_o = 0$ m^{-3} and $e_{11} + e_{33} = 0$ Cm^{-1}. The curve for $n_o = 1.0 \times 10^{20}$ m^{-3} is not shown because this would be coincident with the solid line. Therefore the decrease in the distortion across the layer and the accompanying reduction of the mid-layer tilt due to the effect of the flexoelectric polarisation is virtually cancelled by the shielding effect of the mobile ions at this high number density.

There is a trade-off where higher values of the sum of the flexoelectric coefficients cause the mid-layer tilt angle θ_m to decrease below the zero flexoelectric polarisation value of 1.036 rad, but at higher values of the ionic charge density n_o shielding partially or fully cancels this decrease. This is illustrated in Fig. 5 which shows a surface plot of the value of θ_m as a function of both $e_{11} + e_{33}$ and the base 10 logarithm of n_o for $H/H_c = 1.5$. The value of θ_m is reduced only when the sum of the flexoelectric coefficients is large but the ionic number density is small. Note that for the highest values of $e_{11} + e_{33}$ a value of n_o of 1.0×10^{20} m^{-3} is still insufficient to provide full shielding and return θ_m back up to 1.036 rad. The analytical equations (24) and (25) give an insight, albeit for the region only just above threshold, into how this trade off operates. The second term in (24) has the square of the sum $e_{11} + e_{33}$ in the numerator, but this is acted against by having the term λ^2 in the denominator. From equation(22), λ^2 is directly proportional to the ionic number density, n_o.

Since the square of $e_{11} + e_{33}$ appears in equation (24) then the appearance and effects of the flexoelectric polarisation in this geometry should be independent of the sign of the sum of the flexoelectric coefficients. However at higher fields, where the asymptotic analysis is no longer a good approximation to the full solution to equations (4) to (7), we find that there are small differences in the potential profile and the **n**-director profile between the cases where the sign of $e_{11} + e_{33}$ is positive or negative. These differences would also be seen if the **n**-director distortion in the nematic layer were caused by electric fields of different polarity but with the sign of $e_{11} + e_{33}$ kept constant. Following from this there will be implications for the theoretical treatment of a nematic layer with a flexoelectric polarisation under applied a.c. voltages [12].

Figure 6 shows the results of the numerical calculation of the mid-layer distortion, θ_m, as a function of static magnetic field. All of the curves with different values of $e_{11} + e_{33}$ and n_o take the same value of θ_m up until the Freedericksz threshold, $H/H_c = 1$. Above the threshold there is a sharp increase in the value of θ_m in every case, but the gradients of the curves are different. The solid curve, which shows the steepest gradient immediately above the threshold, is for $n_o = 0$ m^{-3} and $e_{11} + e_{33} = 0$ Cm^{-1}. The lowest gradient occurs when the ionic number density n_o is still zero but the sum of the flexoelectric coefficients is increased to $e_{11} + e_{33} = 3.0 \times 10^{-11}$ Cm^{-1}. The behaviour of the curves with non-zero values of n_o is in accordance with the discussion above, i.e. a high value of n_o tends to provide shielding which cancels the decrease in the value of θ_m caused by the flexoelectric polarisation. An important feature in Fig. 5 is that the curves with different values of $e_{11} + e_{33}$ and n_o are very close

to converging by the time H/H_c has reached a value of 2.5. The curves do not cross as the magnetic field is further increased, but the separation between them decreases further.

In a practical measurement of the Freedeericksz transition either the transmission of light, with the cell between crossed polarisors, or the capacitance of the liquid crystal cell, is monitored as a function of the applied magnetic field [6, 7, 8]. In Fig. 7 we show the permittivity as a function of the relative magnetic field strength, H/H_c, using precisely the same results from the numerical simulations that were used to generate the curves shown in Fig. 6. The permittivity was calculated by dividing the layer into a large number of slices and summing the reciprocals of the z-components of the permittivities of the individual slices using a numerical integration technique. The gradients of the permittivity versus H/H_c curves immediately above the Freedericksz threshold behave in a similar manner to Fig. 6 considering the different values used for the sum of the flexoelectric coefficients, $e_{11}+e_{33}$, and the initial charge number density, n_o. The gradient is reduced when $e_{11}+e_{33} = 3.0\times\ 10^{-11}$ Cm^{-1} as long as the initial charge number density is of order 1.0×10^{19} m^{-3} or below.

When the relative magnetic field strength is above $H/H_c > 1.5$ a different behaviour is observed for the permittivity in Fig. 7 compared to the mid-layer tilt angle in Fig. 6. In Fig. 7 the permittivity curves for which $e_{11}+e_{33} = 3.0 \times 10^{-11}$ Cm^{-1} and n_o takes values 0, 10^{18}, and 10^{19} m^{-3} all converge at high fields. The curve for which the charge number density and sum of the flexoelectric coefficients are zero remains at a higher permittivity above these converged curves. The difference between the observed high field behaviours in Fig. 6 and Fig. 7 arises from the fact that the mid-layer tilt angle only shows the maximum tilt angle at a particular value of H/H_c. The permittivity, however, is calculated from the full **n**-director profile through the layer. As the field is increased the high gradients in the **n**-director, from which the greatest flexoelectric polarisation arises, become more and more localised to the regions near to the boundaries of the cell. The influence of this polarisation on the mid-layer tilt angle therefore becomes proportionately less. However, a given value of the ionic number density becomes less effective in shielding the flexoelectric polarisation in these regions. It is possible that this feature could be helpful in determining the true value of the flexoelectric coefficients of a nematic material, despite any contamination being present.

The Debye screening length [24], defined by $\lambda = (\epsilon\epsilon_o k_B T/n_0 e^2)^{1/2}$, indicates the length over which the mobile charge density n_o will be effective in screening the flexoelectric polarisation due to gradients in the **n**-director. If the flexoelectric polarisation is confined to thin layers near to the boundaries of the cell, as is the case at high values of H/H_c, then the value of λ must be commensurate with widths of the boundary layer to maintain effective screening. This requires higher values of the charge density at the higher values of H/H_c. At a temperature of 300 K and with a permittivity of $\epsilon = 10$, which is between the values of the two components given in Table 1, the Debye screening length takes the values $\lambda = 3.8 \times 10^{-6}$ m when $n_o = 1.0 \times 10^{18}$ m^{-3}, $\lambda = 1.1 \times 10^{-6}$ m when $n_o = 1.0 \times 10^{19}$ m^{-3}, and $\lambda = 3.8 \times 10^{-7}$ m when $n_o = 1.0 \times 10^{20}$ m^{-3}. These values should be considered in the context of the cell

thickness that was used in our simulations, $d = 1.0 \times 10^{-5}$ m. It is clear that a charge density of $n_o = 1.0 \times 10^{18}$ m^{-3} will be insufficient to screen the flexoelectric polarisation at even relatively low values of H/H_c since the corresponding value of λ is approaching half the thickness of the cell.

Another interesting feature that is highlighted by the analytical solution is the dependence of θ_m on the cell thickness d described by equation (24). Although the magnitude of the critical threshold is d-dependent, a plot of θ_m versus H/H_c should not vary with d. Even when flexoelectricity is introduced, inspection of the second term in equation (24) predicts that the cell thickness has no effect unless the charge number density n_o is non zero. These predictions are bourne out by the plots of the mid-layer tilt angle and the permittivity as a function of the relative magnetic field strength H/H_c for different values of the charge number density shown in Figs. (8) and (9). For both of these figures the values of the parameters used are as shown in Table 1 except for the cell thickness, d, and the relative magnetic field strength, H/H_c, which are as indicated. Therefore, for all of the curves shown, relatively high values of the sum of the flexoelectric coefficients and the charge number density are being considered. Under these circumstances the gradient immediately after the threshold field depends upon the cell thickness. Higher cell thicknesses give a steeper gradient, which is in accordance with the prediction of equations (24) and (25). Since all the curves were calculated with the same value $n_o = 1.0 \times 10^{18}$ m^{-3} they all converge at high values of H/H_c for both the mid-layer tilt angle and the permittivity, which is consistent with the numerical results depicted in Figs. (6) and (7).

5 Conclusion

We have shown that the observed influence of a flexoelectric polarisation in the region immediately above the critical magnetic Freedericksz transition can be reduced or even removed by the shielding effects of mobile ionic species having a sufficiently high number density. This effect has been demonstrated in the planar nematic alignment geometry with strong surface anchoring and with equal densities of singly charged positive and negative ionic species. In order for this shielding to occur, higher values of the charge number density n_o are needed for higher values of the sum of the flexoelectric coefficients $e_{11} + e_{33}$. Analytical calculations have given an insight into how the shielding is controlled by the interplay between these parameters and by other variables such as the cell thickness, the elastic constants, the static permittivity tensor for the liquid crystal and the mobilities of the ionic species.

One interesting observation is the differences in the behaviour of the mid-layer tilt as compared to the permittivity as a function of magnetic field when considering different values for the sum of the flexoelectric coefficients and the charge number density. At high magnetic fields the permittivity is reduced by having a non zero value of $e_{11} + e_{33}$ and this reduction remains for number densities up to $n_o = 1.0 \times 10^{20}$ m^{-3}. This suggests the possibility that

measurements at high field could be used to indicate the presence of a flexoelectric polarisation almost independently of the level of ionic contamination in the nematic material. This possibility requires further investigation because the permittivity has been calculated by dividing the nematic layer into thin slices and considering the permittivity tensor in each slice. In a practical measurement a small a.c. voltage would be applied and the capacitance, and thus permittivity, of the layer would be inferred from the relative phase and amplitude of the resultant a.c. displacement current. If the probe voltage is small and its frequency is high then any fluctuations that this causes in the charge density profile and the director distortion and associated flexoelectric polarisation may be negligible. However, it is difficult to achieve high magnetic fields using standard laboratory equipment and so further work is underway to investigate if a similar effect could be observed if the **n**-director distortion is caused by a large a.c. voltage which is also used to measure the capacitance.

References

[1] P. G. DeGennes and J. Prost, *The Physics of Liquid Crystals*, 2nd Edition, Oxford Science Publications (1995)

[2] S. Chandrasekhar, *Liquid Crystals*, 2nd Edition, Cambridge University Press (1992)

[3] R.B. Meyer, Phys Rev Lett **22**, 918 (1969)

[4] J. Prost and J.P. Marcerou, J. Physique **38**, 315 (1977)

[5] M.A. Osipov, J. Physique Lett. **45**, L823 (1984)

[6] V. Freedericksz and V. Zolina, Trans. Faraday Soc. **29**, 919 (1933).

[7] H. Gruler, T.J. Scheffer and G. Meier, Z. Naturforsch **27a**, 966 (1972)

[8] I. Haller, J. Chem. Phys. **57**, 1400 (1972)

[9] M.J. Bradshaw and E.P. Raynes, Mol. Cryst. Liq. Cryst. **72**, 35 (1981).

[10] H.J. Deuling, Solid State Comm. **14**, 1073 (1974)

[11] H.J. Deuling, Mol. Cryst. Liq. Cryst. **26**, 281 (1973)

[12] C.V. Brown and N.J. Mottram, Phys. Rev. E. **68**, 31702 (2003)

[13] A.G. Petrov, chapter 5.5 in *Physical Properties of Liquid Crystals*, I.E.E. Press (2000)

[14] S. Ponti, P. Ziherl, C. Ferrero and S. Zumer, Liquid Crystals **8**, 1171 (1999)

Quantity		Value	Units
Cell thickness	d	1.0	$\times 10^{-5}$ m
Pretilt at boundary	α	1.0	$\times 10^{-10}$ rad
Susceptability anisotropy	$\Delta\chi$	1.5	$\times 10^{-6}$ no unit
Parallel permittivity	$\epsilon_{\parallel}$	19.1	
Perpendicular permittivity	$\epsilon_{\perp}$	5.18	
Sum of flexoelectric coefficients	$e_{11} + e_{33}$	3.0	$\times 10^{-11}$ Cm^{-1}
Splay elastic constant	K_1	11.2	$\times 10^{-12}$ N
Bend elastic constant	K_3	15.7	$\times 10^{-12}$ N
Rotational viscosity	γ_1	0.01	Nsm^{-2}
Electron mobility	μ_e	1.0	$\times 10^{-8}$ $\mathrm{m}^2\mathrm{V}^{-1}\mathrm{s}^{-1}$
Hole mobility	μ_h	1.0	$\times 10^{-8}$ $\mathrm{m}^2\mathrm{V}^{-1}\mathrm{s}^{-1}$
Electron diffusivity	D_e	$0.025\mu_e$	$\mathrm{m}^2\mathrm{s}^{-1}$
Hole diffusivity	D_h	$0.025\mu_h$	$\mathrm{m}^2\mathrm{s}^{-1}$
Charge number density	n_o	1.0	$\times 10^{18}$ m^{-3}
Magnetic field as ratio of critical field	H/H_c	1.5	

Table 1: Default values of the parameters that are used in the numerical calculations.

[15] B. Valenti, C. Bertoni, G.B arbero, P.Taverna-Valabrega, R. Bartolino, Mol. Cryst. Liq. Cryst. **146**, 307 (1987)

[16] J.L. Ericksen, Arch. ration. Mech. Anal. **4**, 231 (1960).

[17] F.M. Leslie, Quart. J. Mech. Appl. Math. **19**, 357 (1966).

[18] Stewart, I.W., *The Static and Dynamic Continuum Theory of Liquid Crystals*, London, Taylor & Francis (2004).

[19] P. Rudquist and S.T. Lagerwall, Liq. Cryst. **23**, 503, (1997).

[20] P. Lorrain, D.R. Corson, and F. Lorrain, *Electromagnetic Fields and Waves*, 3rd Edition, New York, Freeman, (1988).

[21] H.A. Pereira, F. Batalioto and L.R. Evangelista, Phys. Rev. E. **68**, 040701 (2003).

[22] L. Parry-Jones, Private communication (2006).

[23] COMSOL Inc. 1 New England Executive Park, Suite 350, Burlington, MA 01803, USA

[24] J. Israelachvili, *Intermolecular Forces*, London, Academic Press (1985)

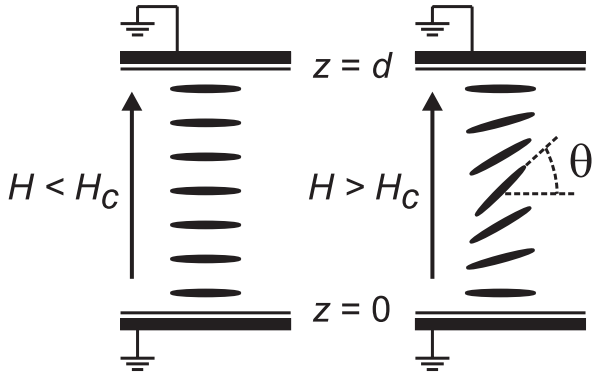

Figure 1: Illustration of the geometry under investigation

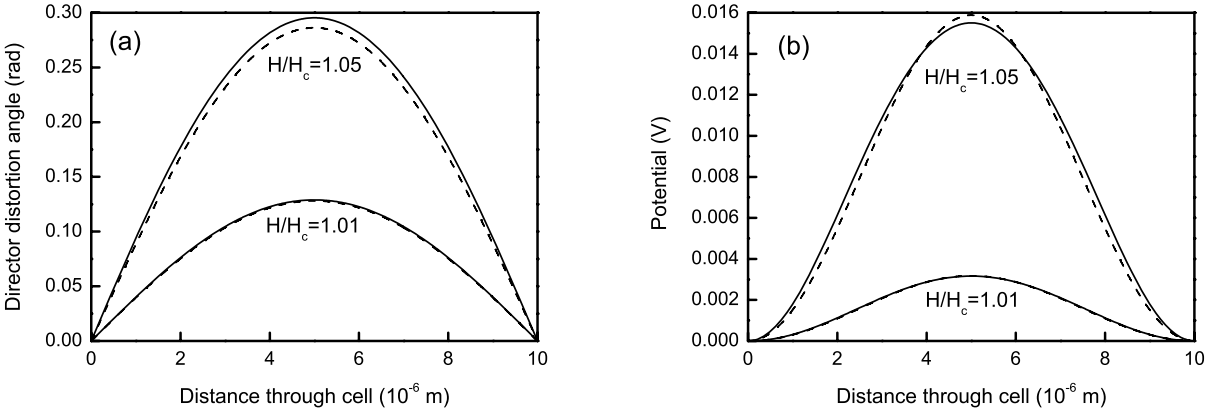

Figure 2: (a) Director distortion and (b) potential across the cell for different applied magnetic fields. The dashed and solid lines represent the analytical and numerical solutions respectively. The parameters used in the calculations are given in Table 1.

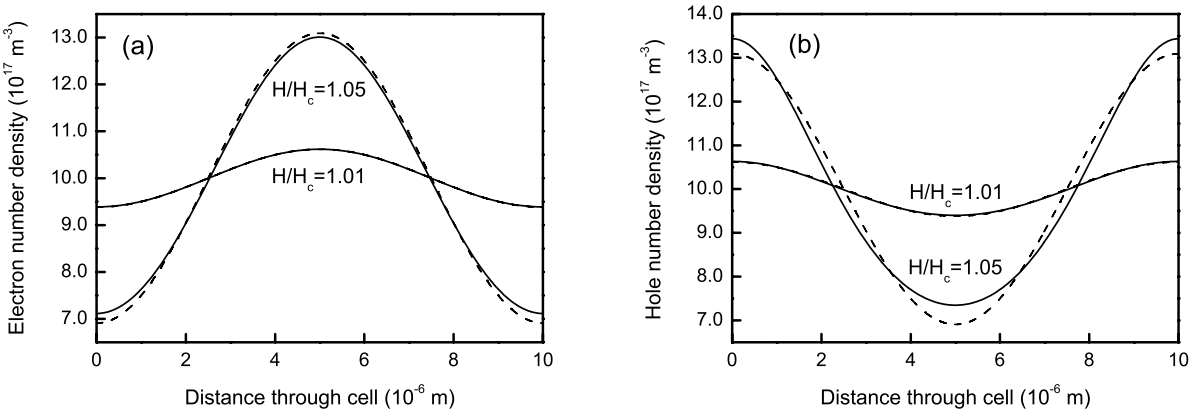

Figure 3: (a) Electron number density and (b) hole number density across the cell for different applied magnetic fields. The dashed and solid curves represent the analytical and numerical solutions, respectively. The parameters used in the calculations are given in Table 1.

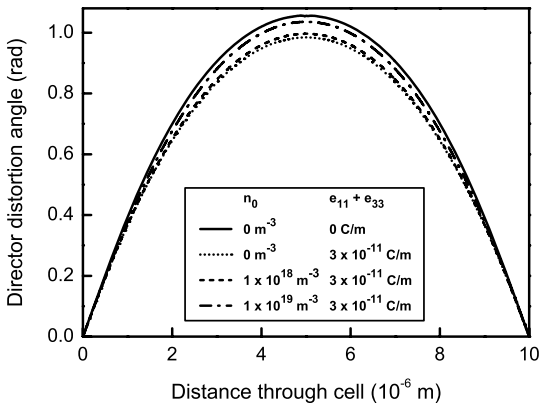

Figure 4: Director distortion across the cell for different initial constant charge number densities and the sum of the flexoelectric coefficients. The parameters used in the numerical calculations are given in Table 1.

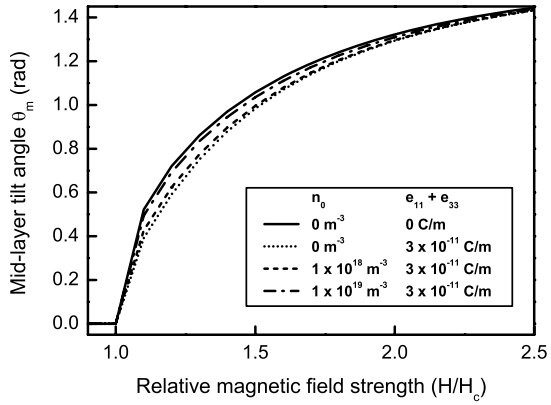

Figure 5: Mid-layer tilt angle as a function of the constant charge number density and sums of the flexoelectric coefficients. The parameters used in the numerical calculations are given in Table 1.

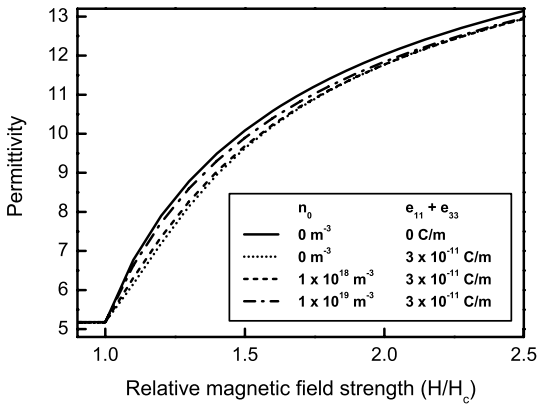

Figure 6: Distortion in the centre of the cell as a function of applied magnetic field for different constant charge number densities and sums of the flexoelectric coefficients. The parameters used in the numerical calculations are given in Table 1.

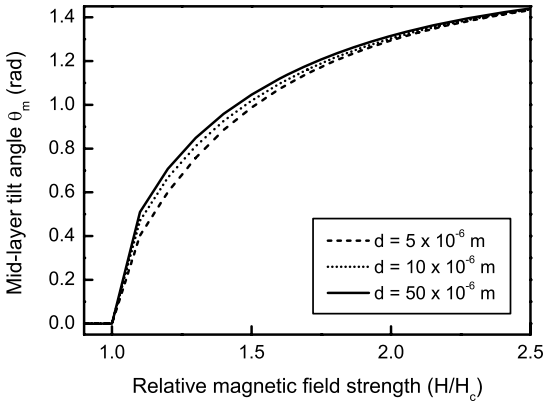

Figure 7: Permittivity of the cell as a function of applied magnetic field for different constant charge number densities and sums of the flexoelectric coefficients. The parameters used in the numerical calculations are given in Table 1.

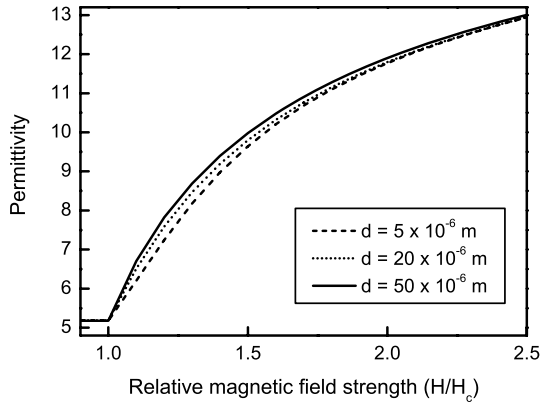

Figure 8: Distortion in the centre of the cell as a function of applied magnetic field for different cell thicknesses. The parameters used in the numerical calculations are given in Table 1.

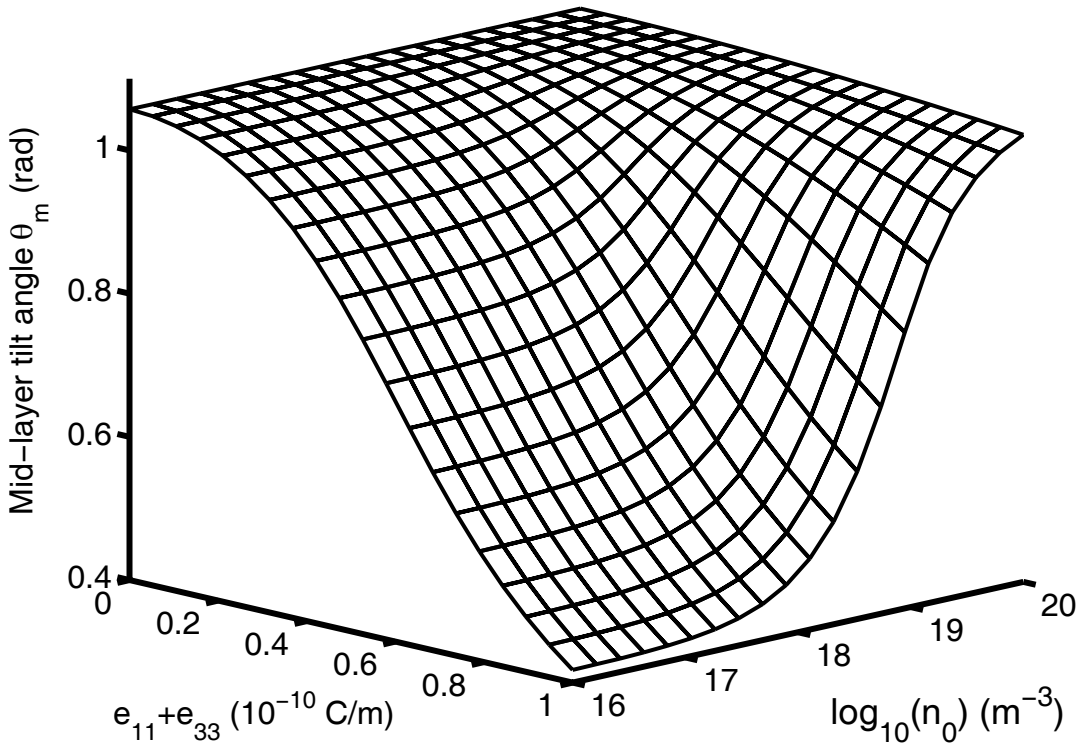

Figure 9: Permittivity of the cell as a function of applied magnetic field for different cell thicknesses. The parameters used in the numerical calculations are given in Table 1.